Supplementary information

Hydrotreatment of Kraft Lignin to Alkylphenolics and Aromatics using Ni, Mo and W Phosphides Supported on Activated Carbon

Ramesh Kumar Chowdari[1,2], Shilpa Agarwal[1,3], Hero Jan Heeres[1]*

[1]Chemical Engineering Department, ENTEG, Faculty of Mathematics and Natural Science, University of Groningen, Nijenborgh 4, 9747 AG Groningen, The Netherlands

[2]Centro de Nanociencias y Nanotecnologia, Universidad Nacional Autonoma de Mexico, Km. 107 CarreteraTijuana-Ensenada, 22800 Ensenada, Baja California, Mexico

[3]Catalytic Processes and Materials, MESA+ Institute for Nanotechnology, Faculty of Science and Technology, University of Twente, P.O. Box 217, 7500 AE Enschede, The Netherlands

*Corresponding author E-mail: h.j.heeres@rug.nl

Number of Pages: 13

Number of Figures: 11

Number of Tables: **5**

FIGURES

Figure S1 Visual appearance of the liquid products after the catalytic hydrotreatment reaction.

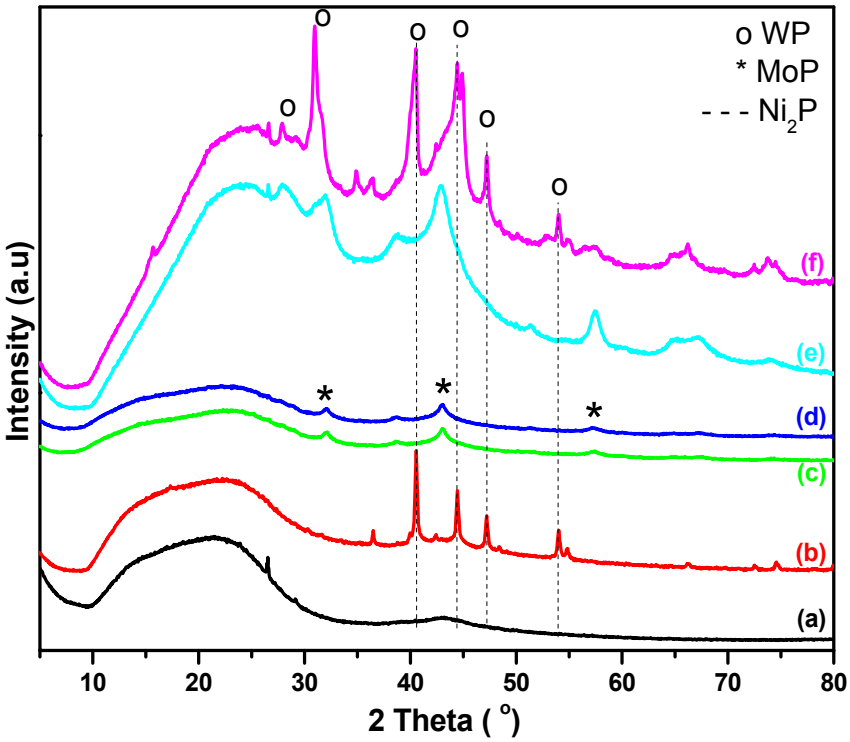

Figure S2 XRD patterns of metal phosphides supported on activated carbon catalysts: (a) AC, (b) 5NiP/AC, (c) 15MoP/AC, (d) 20NiMoP/AC, (e) 15WP/AC, (f) 20NiWP/AC.

The XRD spectra for the monometallic Ni phosphides (5NiP/AC) are in line with literature data and show peaks at 2θ values of 40.67, 44.60, 47.24, 54.03 and 55.13, corresponding to (111), (201), (210)

(300), (002) crystal planes of Ni_2P.[1,2,3] The MoP phase in the monometallic MoP/AC is present at 32.16, 43.00 and 57.30, in line with literature data.[3] In the case of the bimetallic 20NiMoP/AC catalyst, the Ni_2P phase was not observed, which is either due to the presence of highly intense MoP peaks and/or that the nanoparticles are highly dispersed on the AC.[2,3] The XRD spectra for the mono- and bimetallic W containing catalysts (15WP/AC and 20NiWP/AC) show the presence of a WP phase. The peak of the Ni_2P case for the bimetallic catalyst 20NiWP/AC was shown to be overlapping with the WP phase. All XRD data are in line with literature data for catalysts prepared with the same synthesis protocol.[4,5]

Figure S3 shows the TEM image of as prepared 20NiMoP/AC catalyst. A wide range of particles sizes (up to 100 nm size) can be seen. These values are larger than reported for a NiMoP catalyst supported on silica.[3] For the latter, the average particle size was a strong function of the intermediate calcination temperature and values between 11 and 23 nm were reported for a calcination temperature of 700°C, and larger, unspecified ones for 800°C. A possible explanation is the difference in interaction between the nanoparticles and the AC support. A stronger interaction between nanoparticles and silica is expected, reducing the tendency for agglomeration and leading to smaller particles. In addition, in our case the metal loading for the catalyst is higher, which may also lead to larger average nanoparticle sizes.

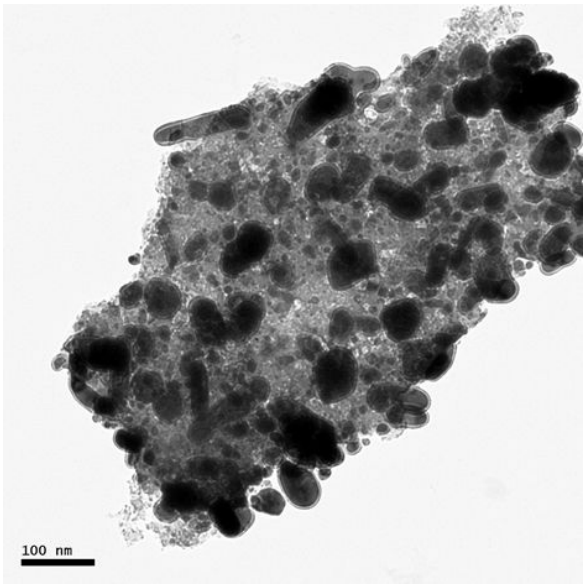

Figure S3 TEM image of the fresh 20NiMoP/AC catalyst

Textural properties of the AC used in this study and the supported metal phosphide catalysts were evaluated by nitrogen physisorption experiments and the results are shown in Table 2 in the main text. The adsorption isotherms of both AC and 20NiMoP/AC exhibited combination of type-I (Langmuir) and type-IV (hysteresis loop) isotherms (Figure S3). This implies that both samples contain micro pores and meso/macro pores.[6] The BET surface areas of the AC and 20NiMoP/AC were calculated to be 752 and 381 m^2/g, respectively. In addition, from the pore size distribution curves, it is clear that there is no significant change in average pore diameter upon loading of metal phosphides. In general, BET surface area decreases on introducing metals and this decrease is significant at high metal loadings. From our results, we can clearly suggest that the metal phosphides are also introduced in the pores, leading to substantial pore (micro/meso) blockage.

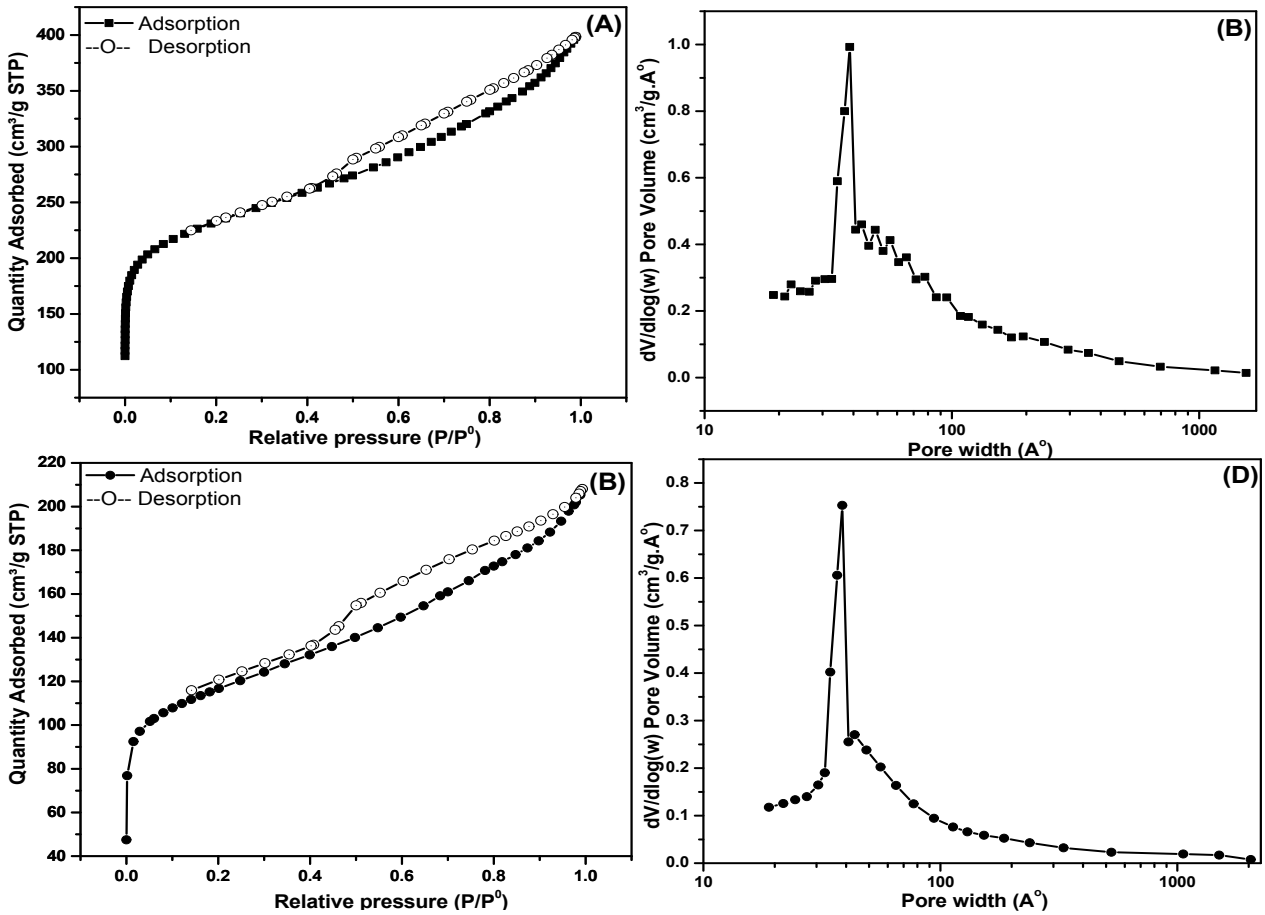

Figure S4 Adsorption isotherms and pore size distribution curves of Activated carbon (A,B) and 20NiMoP/AC catalyst (C,D).

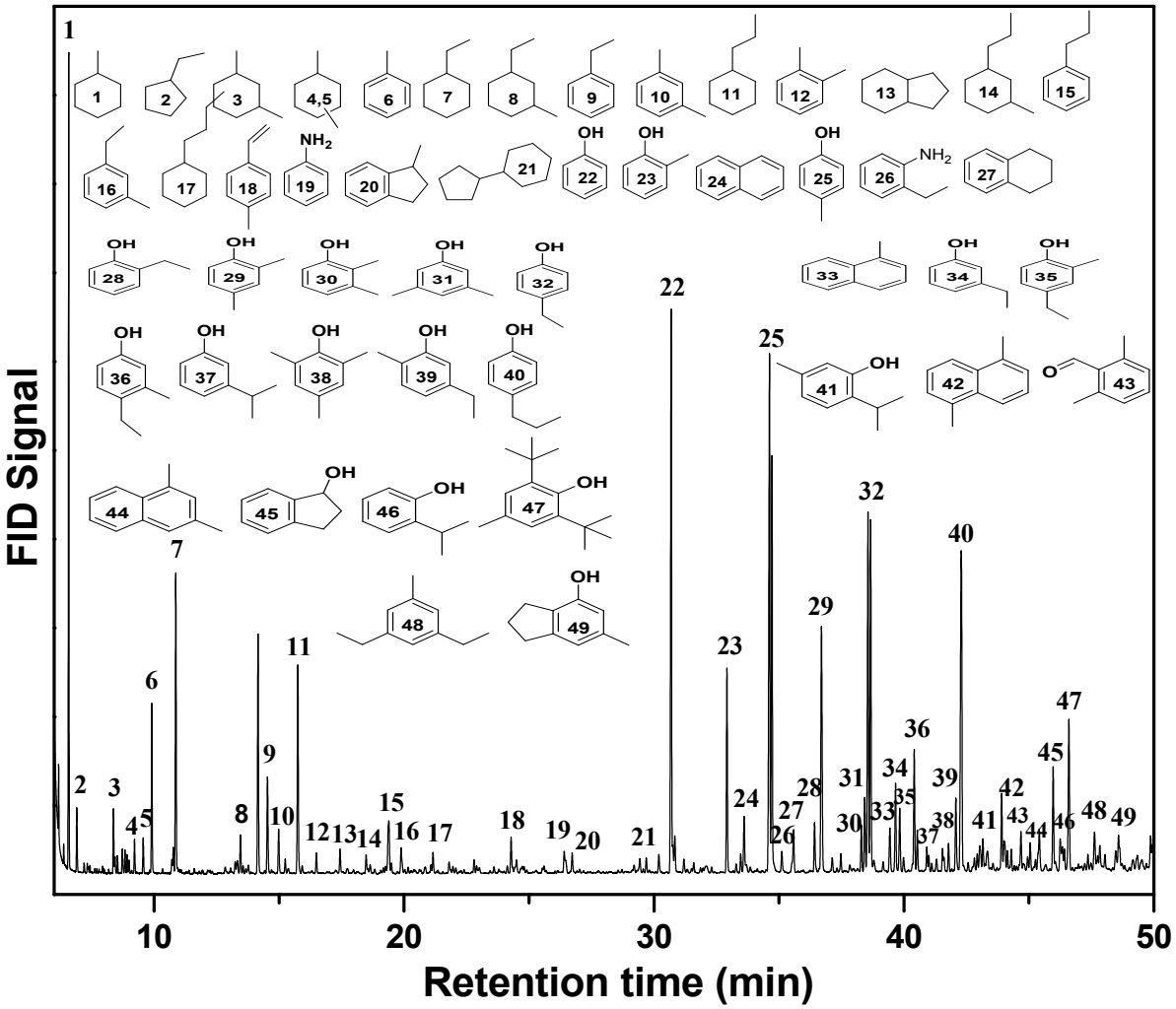

Figure S5 GC-MS of lignin oil obtained for the 20NiMoP/AC at 400 °C.

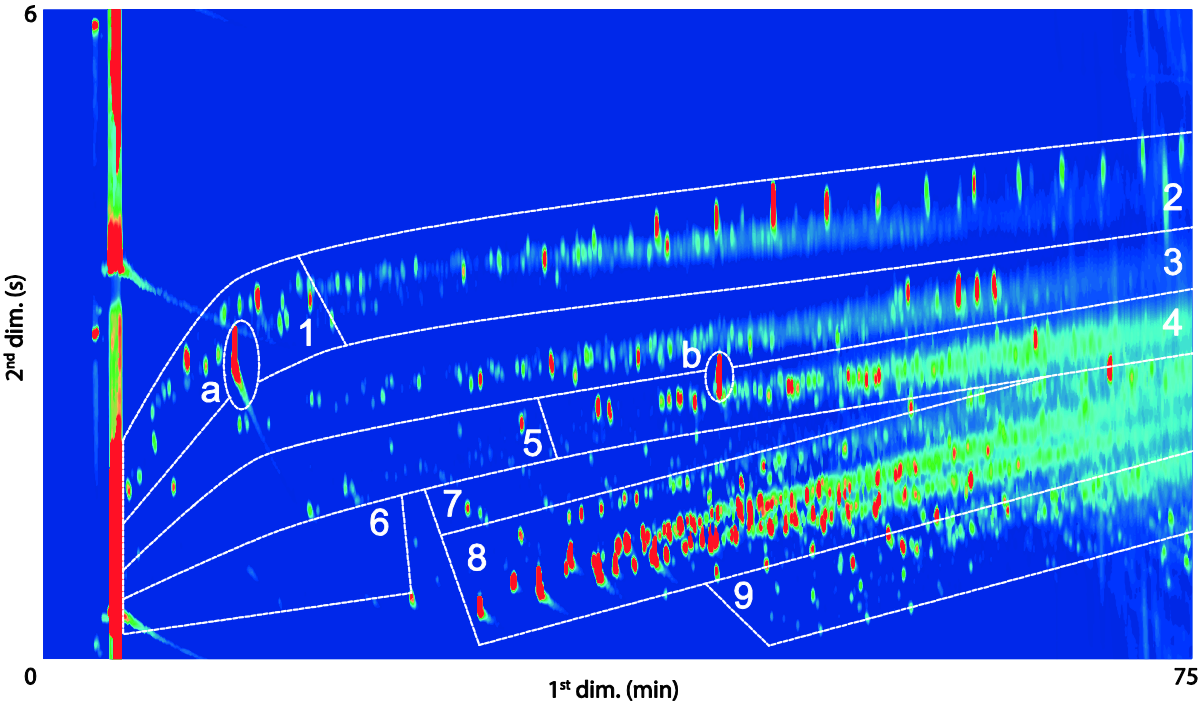

Figure S6 Typical GCxGC chromatogram of hydrotreated Kraft lignin.[7] 1) cyclic alkanes, 2) linear/branched alkanes, 3) aromatics, 4) polycyclic aromatics, 5) ketones/alcohols, 6) acids, 7) guaiacols, 8) alkyl phenolics, 9) catechols, a) internal standard (di-n-butylether), and b) 2,5-di-t-butylhydroxytoluene (stabilizer in THF). (Adapted from ref. 6. Reproduced with permission)

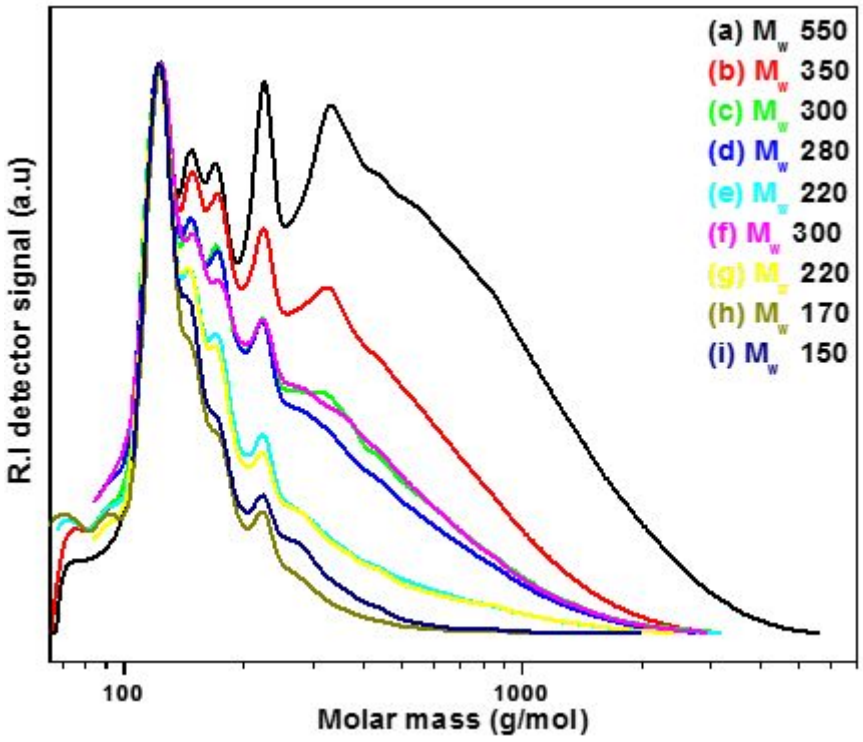

Figure S7 Gel permeation chromatograms of lignin oils obtained for 15MoP/AC at different temperatures and recation times: (a) 400 °C- 0 h, (b) 400 °C- 2 h, (c) 400 °C- 4 h, (d) 400 °C- 8 h, (e) 425 °C- 4 h, (f) 450 °C- 0 h, (g) 450 °C- 1 h, (h) 450 °C- 4 h, and (i) 500 °C- 0 h.

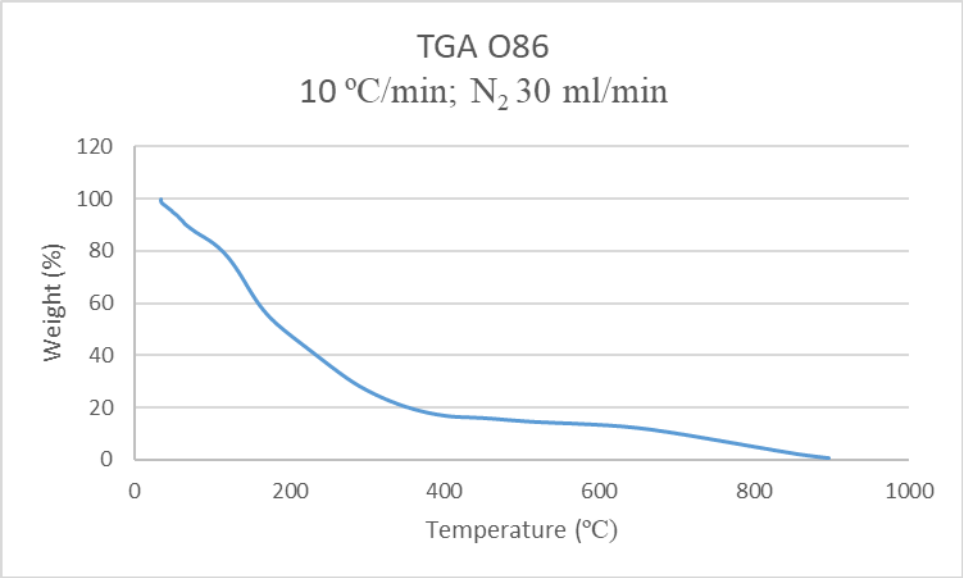

Figure S8. TGA analysis of the liquid phase obtained at 400°C, 100 bar and 10 wt% catalyst loading

TABLES

Table S1 Mass balance for a representative run with 20NiMoP/AC including hydrogen consumption.[a]

roduct	**5% catalyst loading[b]**
Lignin oil (Organic phase)	10.08 (67.2)
Water (Aqueous phase)	2.95 (19.7)
Gas phase	1.29 (8.6)
Solid Residue	0.6, (4)
Total (excluding H_2 consumption)	14.92 (99.5)
Hydrogen consumption	0.53 (3.5)
Grand Total (including H_2 consumption)	15.45 (103)

[a]Reaction conditions: Kraft lignin, 15 g; intake hydrogen pressure of 100 bar at RT; 2 h; 1200 rpm
[b]values in parenthesis are % on wt. basis of lignin intake

Table S2: Gas phase compostion for experimenst carried out at 400°C and 4 h batchtime (Table 3 data)[a]

Catalyst	**T (°C)**	**Time (h)**	**CH_4 (%)**	**C_2H_6 (%)**	**C_3H_8 (%)**	**CO (%)**	**CO_2 (%)**	**Total (%)**
5NiP/AC	400	4	3.6	0.9	0.6	0.2	4.1	9.4
15WP/AC	400	4	4.4	0.8	0.6	0.1	3.6	9.5
20NiWP/AC	400	4	4.6	0.9	0.7	0.1	4.0	10.3
15MoP/AC	400	4	4.4	0.7	0.5	0.1	2.7	8.4
20NiMoP/AC	400	4	5.3	0.8	0.5	0.1	3.4	10.1

[a]All data are wt% based on lignin intake.

Table S3 Coefficients for the regression model for oil yield

Variable	Oil yield (wt%)
Model	IF
Constant	+177.12617
Temperature (T)	-0.25956
Reaction time (t)	+24.69919
H.t	-0.065219

Table S4 ANOVA data for the oil yield

	SS	DF	MS	F	p-value	R^2 values	
Model	891	3	296	22.8	< 0.0024	R^2	0.93
						$R^2_{adjusted}$	0.89
						$R^2_{predicted}$	0.71

GC×GC-FID calibration for quantification of monomers

The first step in the quantification procedure involved determination of the RRF value for a number of representative model components belonging to the various compound groups (alkylphenolics, aliphatic hydrocarbons, aromatics,). The following equation was used to calculate the RRF for an individual model component:

$$RRF = \frac{C_{IS}.A_c}{C_c.A_{IS}}$$

Where, C_{IS} is the concentration of the internal standard, A_{IS} the area of the internal standard (di-n-butylether, DBE), C_C the concentration of the component C, A_C is the area of the component, and RRF is the relative response factor for compound C.

The RRF value for an individual model component was determined by plotting the ratio C_c/C_{IS} versus the ratio $A_c/A_{IS.}$ In such a plot, (see below), the slope is the RRF value for the individual model component.

Figure S9. Examples for the phenolics (alkylated) group**:**

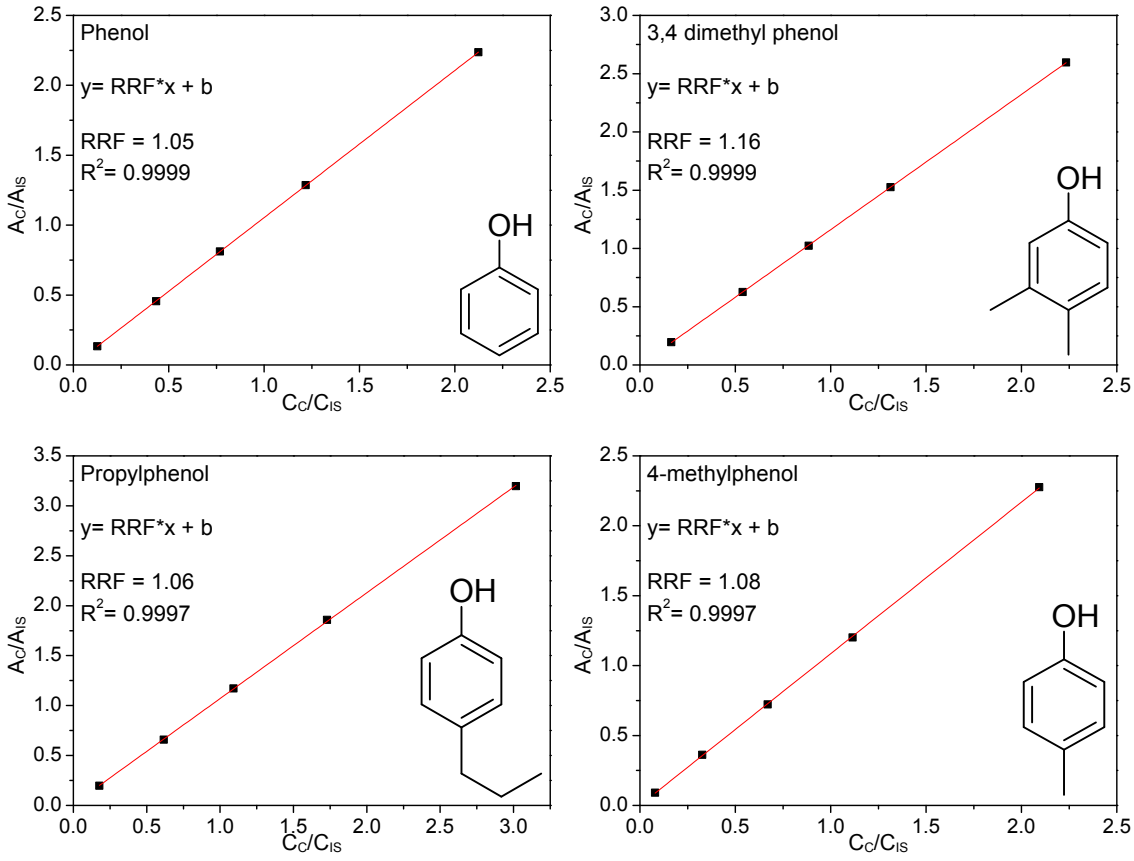

Figure S10. Examples for the guaiacolics (alkylated):

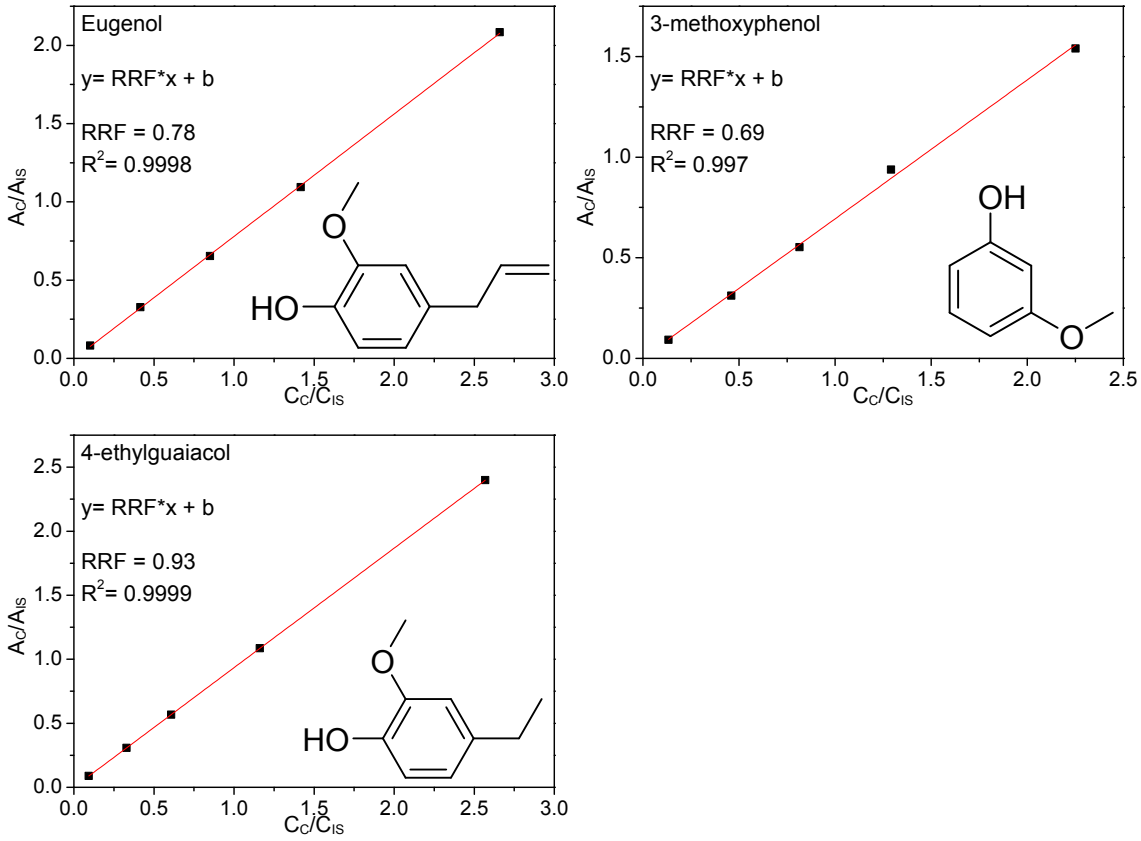

Figure S11. Examples for the aromatics**:**

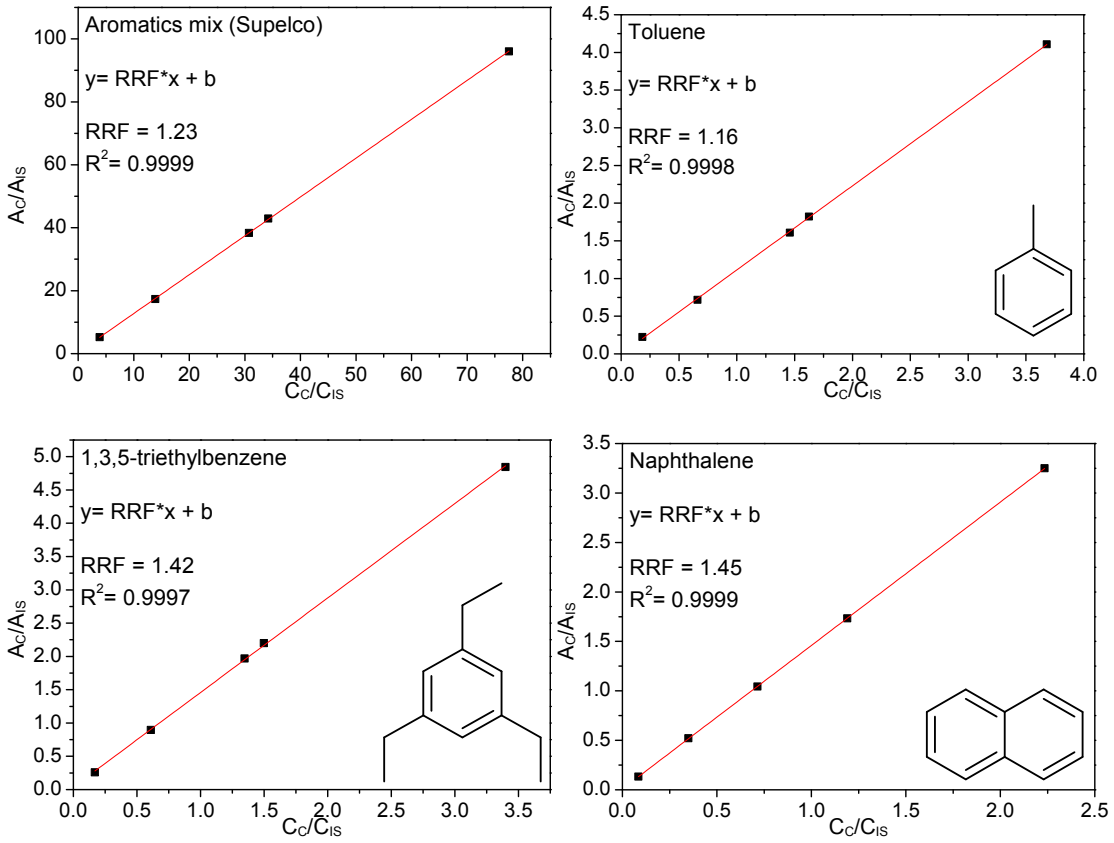

For the quantification based on compound groups, the total compound group area was calibrated over a concentration range of 10 to 100 mg/kg by using 5 calibration mixtures. From these calibrations, an average RRF is calculated for each compound group, see Table S5 below.

Compound group	**RRF (DBE)**
Alkylatedphenolics	1.1
Methoxylated alkylated phenolics	0.9
Polyaromatics/Naphthalenes	1.23
Linear/branched alkanes	1.6
Cyclic alkanes	1.5
Ketones/Alcohols	1

References for Supplementary information

(1) Wu, S.K.; Lai, P.C.; Lin, Y.C.; Wan, H.P.; Lee, H.T.; Chang, Y.H. Atmospheric Hydrodeoxygenation of Guaiacol over Alumina-, Zirconia-, and Silica-Supported Nickel Phosphide Catalysts. ACS Sustain. Chem. Eng. 1(3), **2013**, 349-358.

(2) Ma, D.; Xiao, T.; Xie, S.; Zhou, W.; Cortes, S.L.G.; Green, M.L.H. Synthesis and Structure of Bimetallic Nickel Molybdenum Phosphide Solid Solutions. Chem. Mater. **2004**, 16, 2697-2699.

(3) Pan, Z.; Wang, R.; Li, M.; Chu, Y.; Chen, J. Deoxygenation of methyl laurate to hydrocarbons on silica-supported Ni-Mo phosphides: Effect of calcination temperatures of precursor. Journal of Energy Chemistry 2015, 24, 77-86.

(4) Ma, X.L.; Tian, Y.; Hao, W.Y.; Ma, R.; Li, Y.D. Production of phenols from catalytic conversion of lignin over a tungsten phosphide catalyst. Appl. Catal. A **2014**, 481, 64-70.

(5) Clark, P.; Li, W.; Oyama, S.T. Synthesis and Activity of a New Catalyst for Hydroprocessing: Tungsten Phosphide. J. Catal. **2001**, 200, 140-147.

(6) Balbuenat, P.B.; Gubbins, K.E.; Theoretical interpretation of adsorption behavior of simple fluids in slit pores. Langmuir 1993, 9(7), 1801-1814**.**

(7) Ramesh Kumar, Ch.; Anand, N.; Kloekhorst, A.; Cannilla, C.; Bonura, G.; Frusteri, F.; Barta, K.; Heeres, H.J. Solvent free depolymerization of Kraft lignin to alkyl-phenolics using supported NiMo and CoMo catalysts. Green Chem. **2015**, 17, 4921-4930.